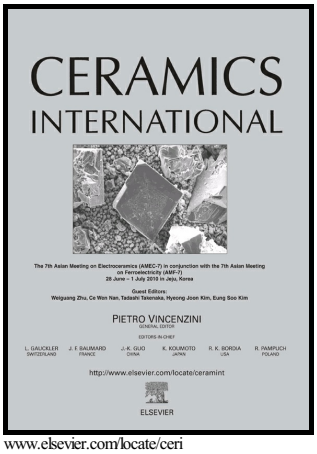

www.elsevier.com/locate/ceri

Structural, thermal and microwave dielectric properties of the novel microwave material $Ba_2TiGe_2O_8$

Huaicheng Xiang, Yang Bai, Chunchun Li, Liang Fang, Heli Jantunen

PII: S0272-8842(18)30692-8
DOI: https://doi.org/10.1016/j.ceramint.2018.03.127
Reference: CERI17764

To appear in: *Ceramics International*

Received date: 2 March 2018
Revised date: 13 March 2018
Accepted date: 14 March 2018

Cite this article as: Huaicheng Xiang, Yang Bai, Chunchun Li, Liang Fang and Heli Jantunen, Structural, thermal and microwave dielectric properties of the novel microwave material $Ba_2TiGe_2O_8$, *Ceramics International,* https://doi.org/10.1016/j.ceramint.2018.03.127

Structural, thermal and microwave dielectric properties of the novel microwave material $Ba_2TiGe_2O_8$

Huaicheng Xiang[1,2*], Yang Bai[2], Chunchun Li[1,3], Liang Fang[1*], Heli Jantunen[2]

[1]*Ministry-province jointly-constructed cultivation base for state key laboratory of Processing for non-ferrous metal and featured materials, Key laboratory of new processing technology for nonferrous metals and materials ministry of education, College of Materials Science and Engineering, Guilin University of Technology, 541004, Guilin, China*

[2]*Microelectronics Research Unit, Faculty of Information Technology and Electrical Engineering, University of Oulu, FI-90014 Oulu, Finland*

[3]*Materials Research Institute, Pennsylvania State University, University Park, PA 16802, USA*

Huaicheng.Xiang@oulu.fi

xianghuaicheng@126.com

fanglianggl001@aliyun.com

[*]Corresponding authors.

Abstract

Rapid developments of microwave dielectric materials have emerged in recent years due to their wide-spread applications and the revolution in wireless communications. However, many commercial microwave materials are based on

titanates, niobates and tantalates which have the disadvantages both of costly raw materials and high sintering temperatures. These result in a production process which is not energy efficient. In this paper we develop a $BaO\text{-}TiO_2\text{-}GeO_2$ ternary system derived from the $BaO\text{-}TiO_2$ binary system to obtain low temperature co-fired microwave dielectric ceramics for high frequency applications. The $Ba_2TiGe_2O_8$ ceramics were prepared via the conventional solid-state route. The X-ray diffraction results showed that $Ba_2TiGe_2O_8$ belongs to the orthorhombic, *Cmm2* space group. The ceramics exhibited a densification of 96.3% after being sintered at 1060 °C. They also exhibited a relative permittivity (ε_r) of 12.7, a quality factor ($Q\times f$) of 9,060 GHz (at 10 GHz), a temperature coefficient of resonant frequency (τ_f) of –30 ppm/°C and a coefficient of thermal expansion (CTE) of 11.0 ppm/°C. In addition, the Raman spectra and ionic polarizability of $Ba_2TiGe_2O_8$ unit cells were investigated.

Keywords: $BaO\text{-}TiO_2\text{-}GeO_2$, Crystal structure, Low-temperature sintering, Microwave dielectric properties, Raman spectra

1. Introduction

Barium oxide-titanium dioxide ($BaO\text{-}TiO_2$) is one of the most popular dielectric materials for industrial applications. This material exhibits both high relative permittivity ($\varepsilon_r > 35$) [1] and low dielectric loss ($\tan\delta < 2\times10^{-3}$) [2]. These properties are suitable for applications in microwave components such as mobile phones, the internet of things (IoT) and intelligent transport systems (ITS), etc [3-6]. However, the fabrication of the $BaO\text{-}TiO_2$ binary system requires a high sintering temperature (>

1300 °C). In addition, $BaO\text{-}TiO_2$ exhibits a large temperature coefficient of resonant frequency (τ_f), which limits its thermal stability as well as its compatibility for integration with low melting point materials [7,8]. For instance, in order to enable low temperature co-fired ceramic (LTCC) packages, the sintering temperature of the dielectric materials should be lower than the melting point of the electrodes – such as silver (960 °C) or copper (1085 °C) [9-11].

Recently, germanium-containing microwave dielectric ceramics, such as $Bi_2Ge_3O_9$ [12], $Li_2ZnGe_3O_8$ [13] and Li_2AGeO_4 (A = Zn, Mg) [14], have attracted much attention. Due to the introduction of Ge, a lower sintering temperature can be achieved in these materials compared to that of the $BaO\text{-}TiO_2$ compounds. For instance, Li_2AGeO_4 (A = Zn, Mg) can be sintered at 1100 °C. Meanwhile, its microwave-range dielectric properties are considered to be suitable for high frequency devices because of the low relative permittivity (6.1-6.5) [14]. Accordingly, in this paper we extend the $BaO\text{-}TiO_2$ binary system to a $BaO\text{-}TiO_2\text{-}GeO_2$ ternary system. With this system, low temperature co-fired microwave dielectric ceramics for high frequency applications may be expected. $Ba_2TiGe_2O_8$, which belongs to the $BaO\text{-}TiO_2\text{-}GeO_2$ group, is investigated. $Ba_2TiGe_2O_8$ has a layered structure whose unit cells belong to the space group of *Cmm2*. With good values of polarizability, piezoelectricity and pyroelectricity, the potential applications of $Ba_2TiGe_2O_8$ could include ferroelectric devices, second harmonic generators and femtosecond lasers [15-18]. The structure of $Ba_2TiGe_2O_8$ has been reported by Iijima *et al* [19]. However, the relationship between the crystal structure and the microwave-range dielectric

properties have not been clarified. This paper focuses on the investigation of such issues, using $Ba_2TiGe_2O_8$ ceramics fabricated at various sintering temperatures. In addition, the Raman spectra, sintering behavior, microstructure and thermal properties of the $Ba_2TiGe_2O_8$ ceramics are studied.

2. Experimental

2.1. Synthesis and Fabrication

The conventional solid-state route was used to synthesize and fabricate the $Ba_2TiGe_2O_8$ powder and ceramics. $BaCO_3$ (> 99%, Alfa Aesar GmbH & Co KG, Germany), TiO_2 (> 99.9%, Alfa Aesar GmbH & Co KG, Germany) and GeO_2 (> 99.99%, Alfa Aesar GmbH & Co KG, Germany) were used as the reactants. They were weighed according to the stoichiometry and then mixed by ball milling for 4 h using zirconia balls, a polyethylene jar as the container and ethanol as the vehicle. After drying at 100 °C, the mixture of the reactants was loaded into an Al_2O_3 crucible and calcined at 1000 °C for 4 h in air. The calcined powder was then ball milled again for 4 h using the same procedure as above to reduce the particle size. The calcined, milled and dried (at 100 °C) powder was mixed with the binder – 5 wt % polyvinyl alcohol (5 wt %, water as the solvent) - and uniaxially pressed into green body disks (10 mm in diameter and 5 mm in thickness) and cylindrical samples (5 mm in diameter and 12 mm in length) under a pressure of 100 MPa. The binder was burnt off at 550 °C for 2 h (ramping rate of 1.5 °C/min). The disks were finally sintered at 1000-1080 °C for 4 h in air with a heating rate of 5 °C/min.

2.2. Characterization

The mixture of the reactants was assessed by Thermogravimetric Analysis (TGA) and Differential Scanning Calorimetry (DSC) with an STA 499 F3 Jupiter (NETZSCH, Germany). The crystal structure of the samples was analyzed by X-ray powder diffraction (XRD, Bruker D8, Germany) with a Cu Kα radiation source. The Raman spectra of the samples were obtained using a Raman spectrometer (Thermo Fisher Scientific DXR, USA). The density of the samples was measured by the Archimedes method. The microstructural images of the polished and thermally etched samples (at 980 °C for 10 min) were obtained by field emission scanning electron microscopy (FESEM, Zeiss Ultra Plus, Germany). The permittivity (ε_r) and quality factor values ($Q\times f$) were measured using the Hakki-Coleman method in which the samples were connected to a vector network analyzer (10 MHz-20 GHz, ZVB20, Rohde & Schwarz, Germany). The τ_f values in the range of 25-85 °C were measured in a temperature chamber (SU261, ESPEC, Japan) and using the same vector network analyzer. All of the above characterizations were carried out with the disc samples. The cylindrical samples were used to measure the coefficient of thermal expansion (CTE) using a dilatometer (DIL 402 PC/4, NETZSCH, Germany) with a heating rate of 5 °C/min and in the range of 25-600 °C.

3. Results and discussions

3.1. Synthesis and crystal structure of $Ba_2TiGe_2O_8$

The TGA/DSC curves of the $Ba_2TiGe_2O_8$ are shown in Figure 1. Obvious endothermic peaks in the DSC curve between 700 °C to 1000 °C were observed, with the corresponding mass loss about 12.6% shown on the TGA curve. This is attributed

to the chemical reaction of the reactants (i.e. $BaCO_3$, TiO_2 and GeO_2) and this process is accompanied by the release of carbon dioxide. When the temperature was higher than 1160 °C, the DSC curve showed two stronger endothermic peaks, which corresponded to the thermal decomposition of $Ba_2TiGe_2O_8$ [18,20].

Figure 2 shows the Rietveld refined XRD pattern and the unit cells of the $Ba_2TiGe_2O_8$. The refinement parameters of $Ba_2TiGe_2O_8$ (R_p = 7.19 %, R_{exp} = 9.52 % and R_{wp} = 3.94 %) showed good results. The $Ba_2TiGe_2O_8$ was analyzed to be an orthorhombic phase (space group *Cmm2*) with lattice parameters of a = 12.2599(1) Å, b = 12.2802(3) Å, c = 5.3642(1) Å, $\alpha = \beta = \gamma$ = 90.0000° and V = 807.6060(1) $Å^3$. Table 1 summarizes the refined atomic coordinates and the reliability factors. The $Ba_2TiGe_2O_8$ structure consisted of a four-coordinate germanium site exhibiting [GeO_4] tetrahedrons and a five-coordinate titanium site forming square pyramidal geometries [TiO_5]. Layered structures were formed from the tetrahedrons and square pyramids separated by the barium residing in the center of the ten-coordinate site [19].

3.2. Raman spectra of $Ba_2TiGe_2O_8$

The Raman spectrum of the $Ba_2TiGe_2O_8$ ceramic sintered at the optimum densification temperature of 1060 °C in the range of 150-950 cm^{-1} is shown in Figure 3. The 75 Raman active modes ($21A_1 + 14A_2 + 20B_1 + 20B_2$) were calculated from the orthorhombic structure with space group *Cmm2*. However, the 22 Raman active modes of $Ba_2TiGe_2O_8$ were fitted by the Lorentz mode, which had much fewer modes than the calculated ones, probably because various peaks overlapped with one another [21]. Because of the stronger covalence of the Ti-O bonds, the stretching vibrations

were shifted to higher wave numbers, leading to a more significant mixing of the Ge-O and Ti-O vibrations. Therefore, the modes with the higher wave number in the Raman spectrum of $Ba_2TiGe_2O_8$ could be those of the Ge-O-Ge bond [22-24]. The five-fold coordinated titanium is the majority species present in the $Ba_2TiGe_2O_8$, as revealed by the strongest band in the spectrum at 843 cm^{-1}. The bands in the range of 700–950 cm^{-1} were assigned to the stretching of the Ti-O bonds. The 548 cm^{-1} was assigned to the υ(Ge-O-Ge) vibration mode and the peaks around 298 cm^{-1} were due to the υ(Ba–O) mode.

3.3. Sintering and densification

Figure 4 shows the FESEM (field emission scanning electron microscopy) images of the polished and thermally etched samples of the $Ba_2TiGe_2O_8$ sintered at 1000-1080 °C. Grain growth is one of the most important factors for densification in the sintering process. In the figure it can be seen that the grain sizes of the $Ba_2TiGe_2O_8$ ceramics were positively related to the sintering temperature, i.e. the higher the sintering temperature the larger the grain size. When sintered at 1000 °C the grain sizes were relatively small (~ 2 μm) (Figure 4 (a)). Some pores could also be seen. When the sintering temperature increased to 1060 °C the $Ba_2TiGe_2O_8$ sample exhibited a relatively dense microstructure with an average grain size of 6 μm and few visible pores (Figure 4 (d)). When the sintering temperature increased to 1080°C the grains were overgrown and some pores re-occurred (Figure 4 (e)). This could reduce the density of $Ba_2TiGe_2O_8$ ceramics from that at the optimum point. These results indicate that the appropriate sintering temperature can effectively promote the

densification of the $Ba_2TiGe_2O_8$ ceramics.

3.4. Microwave dielectric properties

Figure 5 shows the relative density and ε_r of the $Ba_2TiGe_2O_8$ ceramic samples as a function of sintering temperature. The relative density increased with sintering temperature until 1060 °C, then slightly decreased due to over-heating, which corresponded to the FESEM image shown in Figure 4 (e). The variation of ε_r values showed a trend similar to that of the relative density. It indicates that density plays an important role in the microwave dielectric properties. The $Ba_2TiGe_2O_8$ ceramics sintered at 1060 °C with the highest densification of 96.3 % showed the optimum ε_r of 12.7 at the measured frequency (10 GHz). Because the porosity in the sintered ceramics influences the ε_r values, the measured ε_r should be corrected to the actual permittivity [25]. This correction can be performed with the Bosman and Havinga method, as expressed in Equation 1 [26].

$$\varepsilon_{corr.} = \varepsilon_m (1 + 1.5p) \quad (1)$$

In the equation, p, $\varepsilon_{corr.}$ and ε_m are the fractional porosity and the corrected and measured values of permittivity, respectively. The $\varepsilon_{corr.}$ value was about 13.4 (± 0.2) for the $Ba_2TiGe_2O_8$ ceramics sintered at 1060 °C. In addition to the influence of the density, the permittivity is also affected by the ionic polarizability [27]. The theoretical permittivity (ε_{th}) can be given by the Clausius-Mossotti equation (Equation 2) [28].

$$\varepsilon_{th} = \frac{3V + 8\pi\alpha}{3V - 4\pi\alpha} \quad (2)$$

$$\alpha(Ba_2TiGe_2O_8) = 2\alpha(Ba^{2+}) + \alpha(Ti^{4+}) + 2\alpha(Ge^{4+}) + 8\alpha(O^{2+}) \quad (3)$$

In the equation, V is the cell volume and α is the ionic polarizability. $\alpha(Ba^{2+})$, $\alpha(Ti^{4+})$, $\alpha(Ge^{4+})$, and $\alpha(O^{2+})$ are 6.40 Å^3, 7.28 Å^3, 1.63 Å^3 and 2.01 Å^3, respectively, as shown in Equation 3 [28]. Considering the effect of polarizability, the theoretical permittivity of the $Ba_2TiGe_2O_8$ ceramics was calculated to be 14.1, which is extremely close to the corrected value but higher than the measured value. The relative error between the measured and theoretical permittivity for the $Ba_2TiGe_2O_8$ ceramics was 9.9 %.

Figure 6 shows the variation of $Q\times f$ and τ_f of the $Ba_2TiGe_2O_8$ ceramics with different sintering temperatures. The $Ba_2TiGe_2O_8$ ceramics exhibited a $Q\times f$ value of 9,060 GHz (tan $\delta = 1.1\times10^{-3}$) at a frequency of 10 GHz after sintering at 1060 °C for 4 hours. The τ_f values of the $Ba_2TiGe_2O_8$ ceramics changed slightly from -31.6 to -30.8 ppm/°C when the sintering temperature was increased from 1000 °C to 1080 °C (around -30 ppm/°C for 1060 °C).

The τ_f is related to the temperature coefficient of relative permittivity (τ_ε) and the coefficient of thermal expansion (CTE), as given in Equation 4 [29].

$$\tau_f = -\left(\frac{\tau_\varepsilon}{2} + CTE\right) \quad (4)$$

Figure 7 shows the linear thermal expansion curve in the temperature range of 25−600 °C for the $Ba_2TiGe_2O_8$ ceramics sintered at 1060 °C. The CTE values showed a linear variation with the increase of temperature. An average CTE value of 11.0 ppm/°C was obtained. The $Ba_2TiGe_2O_8$ ceramics exhibited almost uniform CTE values in both the heating and cooling cycles. The temperature coefficient of relative

permittivity (τ_ε) was calculated to be 38 ppm/°C.

The sintering temperatures and microwave dielectric properties of $Ba_2TiGe_2O_8$ and BaO-TiO_2 microwave ceramics are compared in Table 2. Generally, the BaO-TiO_2 ceramics have high permittivities, high $Q\times f$ values and positive τ_f values. It can be seen that the sintering temperature and permittivity of $Ba_2TiGe_2O_8$ were lower than those of the BaO-TiO_2 system ceramics. Therefore, it can be concluded that $Ba_2TiGe_2O_8$ ceramic is the more suitable for increasing the electronic signal transmission and integration of circuits.

Conclusions

A novel microwave dielectric ceramic, $Ba_2TiGe_2O_8$, has been investigated in the present work. The crystal structure of the $Ba_2TiGe_2O_8$ ceramics belongs to the orthorhombic phase in the *Cmm2* space group. The $Ba_2TiGe_2O_8$ ceramics showed a layered structure consisting of [GeO_4] tetrahedrons and [TiO_5] square pyramids separated by the Ba ions residing in the center of the ten-coordinate site. The optical phonon modes of the $Ba_2TiGe_2O_8$ were very clear and sharp. The orthorhombic $Ba_2TiGe_2O_8$ ceramics presented well-defined modes and the variations of the modes of vibration have been studied in detail. The ceramics sintered at 1060 °C exhibited the optimum relative density of 96.3%, a relatively low permittivity of 12.7, a low dielectric loss of 1.1×10^{-3} (at 10 GHz), a τ_f value of –30 ppm/°C and a CTE of 11.0 ppm/°C. The the Raman spectra and ionic polarizability of the $Ba_2TiGe_2O_8$ ceramics have also been investigated.

Acknowledgments

This work was financially supported by Natural Science Foundation of China (Nos. 51502047, 21561008, and 21761008), the Natural Science Foundation of Guangxi Zhuang Autonomous Region (Nos. 2015GXNSFFA139003, 2016GXNSFBA380134, and 2016GXNSFAA380018), Project of Scientific Research and Technical Exploitation Program of Guilin (2016010702-2), and Innovation Project of Guangxi Graduate Education (YCBZ2017052). Author Y. Bai acknowledges the European Union's Horizon 2020 research and innovation program under the Marie Sklodowska-Curie Grant Agreement No. "705437". The authors acknowledges Arthur E. Hill from University of Salford for his help in language improvement.

References

[1]. H.M. O'Bryan, J. Thomson, J.K. Plourde, A new BaO-TiO_2 compound with temperature-stable high permittivity and low microwave loss, J. Am. Ceram. Soc. 57 (1974) 450–453.

[2]. C.L. Huang, C.L. Pan, S.J.n Shium, Liquid phase sintering of $MgTiO_3$–$CaTiO_3$ microwave dielectric ceramics, Mater. Chem. Phys. 78 (2002) 111–115.

[3]. M.T. Sebastian, R. Ubic, H. Jantunen, Microwave materials and applications, Wiley, New York, 2016, pp 653−682.

[4]. T. Tsunooka, M. Androu, Y. Higashida, H. Sugiura, H. Ohsato, Effects of TiO_2 on

sinterability and dielectric properties of high-Q forsterite ceramics, J. Eur. Ceram. Soc. 23 (2003) 2573–2578.

[5]. W.S. Kim, E.S. Kim, K.H. Yoon, Effects of Sm^{3+} substitution on dielectric properties of $Ca_{1-x}Sm_{2x/3}TiO_3$ ceramics at microwave frequencies, J. Am. Ceram. Soc. 82 (2010) 2111–2115.

[6]. W. Lei, W.Z. Lu, J.H. Zhu, X.H. W, Microwave dielectric properties of $ZnAl_2O_4$-TiO_2 spinel-based composites, Mater. Lett. 61 (2007) 4066–4069.

[7]. Y. Chen, S. Duan, S. Zhang, Low temperature sintering kinetics and microwave dielectric properties of $BaTi_5O_{11}$ ceramic. ACS Sustainable Chem. Eng. 5 (2017) 10606–10613

[8]. M.T. Sebastian, H. Jantunen, Low loss dielectric materials for LTCC applications: a review, Int Mater. Rev. 53 (2008) 57–90.

[9]. X.L. Zhu, Z.H. Wang, X.M. Su, P.M. Vilarinho, New Cu_3TeO_6 ceramics: phase formation and dielectric properties, ASC Appl. Mater. Interfaces 6 (2014) 11326−11332.

[10]. J. Guo, D. Zhou, H. Wang, X. Yao, Microwave dielectric properties of (1-*x*)$ZnMoO_4$-*x*TiO_2 composite ceramics, J. Alloys Compd. 509 (2011) 5863–5865.

[11]. G. Zhang, H. Wang, J. Guo, L. He, D. Wei, Q. Yuan, Ultra-low sintering temperature microwave dielectric ceramics based on Na_2O-MoO_3 binary system, J. Am. Ceram. Soc. 98 (2015) 528–533.

[12]. X.H. Ma, S.H. Kweon, S. Nahm, C.Y. Kang, S.J. Yoon, Y.S. Kim, Synthesis

and microwave dielectric properties of $Bi_2Ge_3O_9$ ceramics for application as advanced ceramic substrate, J. Eur. Ceram. Soc. 37 (2017) 605–610.

[13]. H.C. Xiang, L. Fang, W.S. Fang, Y. Tang, C.C. Li, A novel low-firing microwave dielectric ceramic $Li_2ZnGe_3O_8$ with cubic spinel structure, J. Eur. Ceram. Soc. 37 (2017) 625–629.

[14]. C.C. Li, H.C. Xiang, Minyu Xu, Y. Tang, L. Fang, Li_2AGeO_4 (A = Zn, Mg): Two novel low-permittivity microwave dielectric ceramics with olivine structure, J. Eur. Ceram. Soc. 38 (2018) 1524–1528.

[15]. B. Zhu, B. Yu, B. Lu, H. Ma, J. Qiu, Y. Dai, Femtosecond laser-induced oriented precipitation of $Ba_2TiGe_2O_8$ crystals in glass, Opt. Express 16 (2008) 3912–7.

[16]. Y. Takahashi, Y. Benino, T. Fujiwara, T. Komatsu, Formation mechanism of ferroelectric $Ba_2TiGe_2O_8$ and second order optical non-linearity in transparent crystallized glasses, J. Non-Cryst. Solids 316 (2003) 320–330.

[17]. N. Toyohara, Y. Benino, T. Fujiwara, S. Tanaka, K. Uematsu, T. Komatsu, Enhancement and depression in second-order optical nonlinearity of $Ba_2TiGe_2O_8$ in crystallized glass prepared in a high magnetic field, J. Appl. Phys. 99 (2006) 043515.

[18]. X. Liu, L. Huo, B. Liao, Q. Wei, X. Hu, N. Zhuang, J. Chen, L. Huang, G. Zhang, Czochraski growth, defect analysis and refractive index of $Ba_2TiGe_2O_8$ crystal with excellent optical nonlinearities, Opt. Mater. 42 (2015) 361–365.

[19]. K. Iijima, F. Marumo, M Kimura, T. Kawamura, Structure of a ferroelastic

crystal $Ba_2TiGe_2O_8$ and its thermal phase transition, J. Chem. Soc. Jpn. 10 (1981) 1557–1563.

[20]. Y. Kanno, J. Nishino, Effect of hydrolysis water on the crystallization of sol-gel-derived GeO_2, J. Mater. Sci. Lett. 12 (1993) 110–112.

[21]. J. Guo, D. Zhou, L. Wang, H. Wang, T. Shao, Z.M. Qi, X. Yao, Infrared spectra, Raman spectra, microwave dielectric properties and simulation for effective permittivity of temperature stable ceramics $AMoO_4$-TiO_2 (A = Ca, Sr), Dalton Trans. 42 (2013) 1483–1491.

[22]. R. Ogawa, H. Masai, Y. Takahashi, T. Fujiwara, Formation of fresnoite-type $Ba_2TiGe_2O_8$ crystallites in BaO-TiO_2-GeO_2 glass thin film and its optical nonlinearity, J. Ceram. Soc. Jpn. 116 (2008)1130–1133.

[23]. S.A. Markgraf, S.K. Sharma, A.S. Bhalla, Raman study of glasses of $Ba_2TiSi_2O_8$ and $Ba_2TiGe_2O_8$, J. Am. Ceram. Soc. 75 (2010) 2630–2632.

[24]. T.G. Mayerhöfer, H.H. Dunken, Single-crystal IR spectroscopic investigation on fresnoite, Sr-fresnoite and Ge-fresnoite, Vib. Spectrosc. 25 (2001) 185–195.

[25]. M.T. Sebastian, R. Ubic, H. Jantunen, Low-loss dielectric ceramic materials and their properties, Int. Mater. Rev. 60 (2015) 392–412.

[26]. A.J. Bosman, E.E. Havinga, Temperature dependence of dielectric constants of cubic ionic compounds, Phys. Rev. 129 (1963) 1593–600.

[27]. C.L. Huang, S.H. Huang, Low-loss microwave dielectric ceramics in the $(Co_{1-x}Zn_x)TiO_3$ (x = 0-0.1) system, J. Alloys Compd. 515 (2012) 8–11.

[28]. R.D. Shannon, Dielectric polarizabilities of ions in oxides and fluorides, J.

Appl. Phys. 73 (1993) 348–366.

[29]. E.L. Colla, I.M. Reaney, N. Setter, Effect of structural changes in complex perovskites on the temperature coefficient of the relative permittivity, J. Appl. Phys. 74(1993) 3414–3425.

[30]. S.G. Mhaisalker, D.W. Readey, S.A. Akbar, Microwave dielectric properties of doped $BaTi_4O_9$, J. Am. Ceram. Soc. 74 (1991) 1894–1898.

[31]. J.H. Choy, Y.S. Han, J.H. Sohn, M. Itoh, Microwave characteristics of BaO–TiO_2 ceramics prepared via a citrate route, J. Am. Ceram. Soc. 78 (1995) 1169–1172.

[32]. G.H. Maher, C.E. Hutchins, S.D. Ross, Preparation and characterization of ceramic fine powders produced by the emulsion process, J. Mater. Process. Technol. 56 (1996) 200–210.

[33]. M.H. Weng, T.J. Liang, C.L. Huang, Lowering of sintering temperature and microwave dielectric properties of $BaTi_4O_9$ ceramics prepared by the polymeric precursor method, J. Eur. Ceram. Soc. 22 (2002) 1693–1698.

[34]. T. Fukui, C. Sakurai, M. Okayama, Effects of heating rate on sintering of alkoxide derived $BaTi_5O_{11}$ powder, J. Mater. Res. 7 (1992) 192–196.

Fig 1 TGA/DSC curves of the mixture of the reactants (i.e. $BaCO_3$, TiO_2 and GeO_2)

Fig 2 Rietveld refined XRD pattern and schematic of the unit cells of $Ba_2Ge_2TiO_8$.

Fig 3 Measured and fitted Raman spectrum in the range of 150-950 cm^{-1} for the $Ba_2TiGe_2O_8$ sintered at 1060 °C.

Fig 4 FESEM images of the polished and thermally etched $Ba_2TiGe_2O_8$ samples sintered at: (a) 1000 °C, (b) 1020 °C, (c) 1040 °C, (d) 1060 °C, (e) 1080 °C.

Fig 5 Dependence of relative density and ε_r on sintering temperature for the $Ba_2TiGe_2O_8$ ceramics.

Fig 6 Dependence of $Q\times f$ and τ_f on sintering temperature for the $Ba_2Ge_2TiO_8$ ceramics measured at 10 GHz.

Fig 7 Dependence of thermal expansion on temperature for the $Ba_2Ge_2TiO_8$ ceramics sintered at 1060 °C.

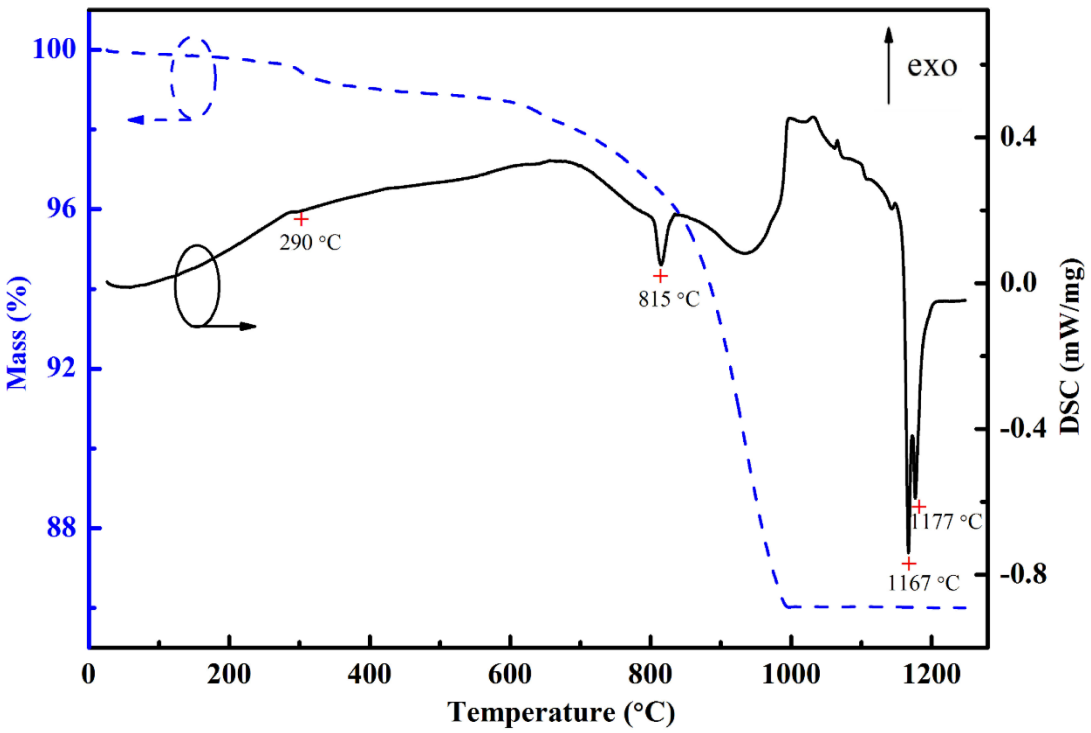

Figure 1

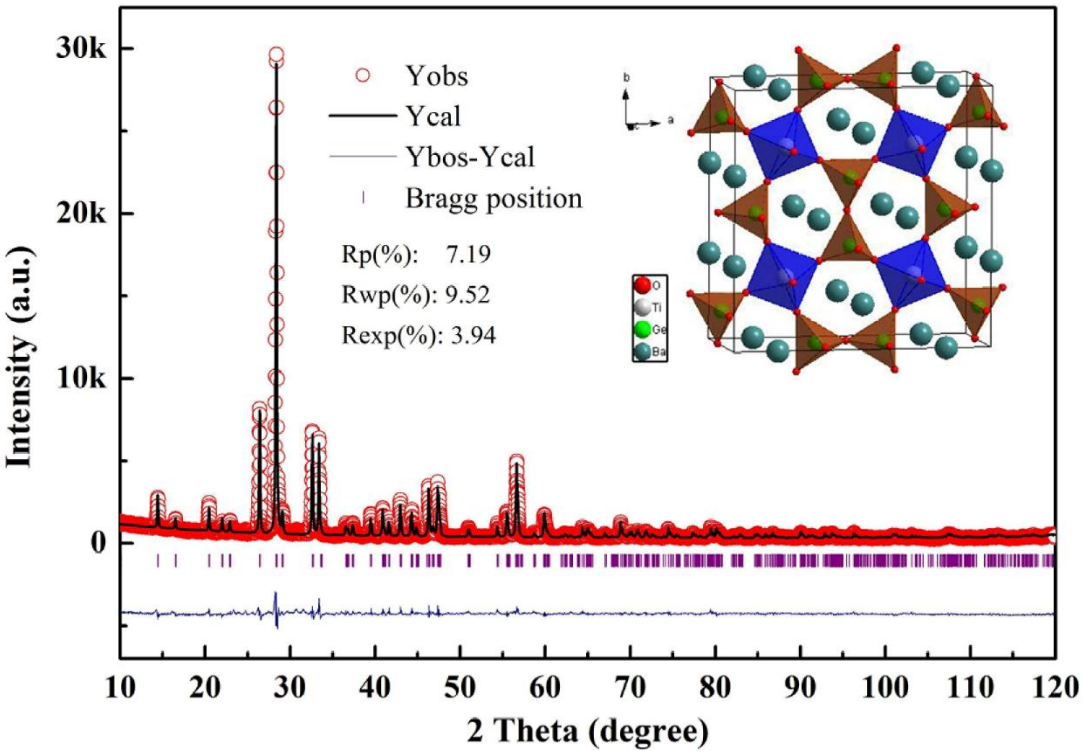

Figure 2

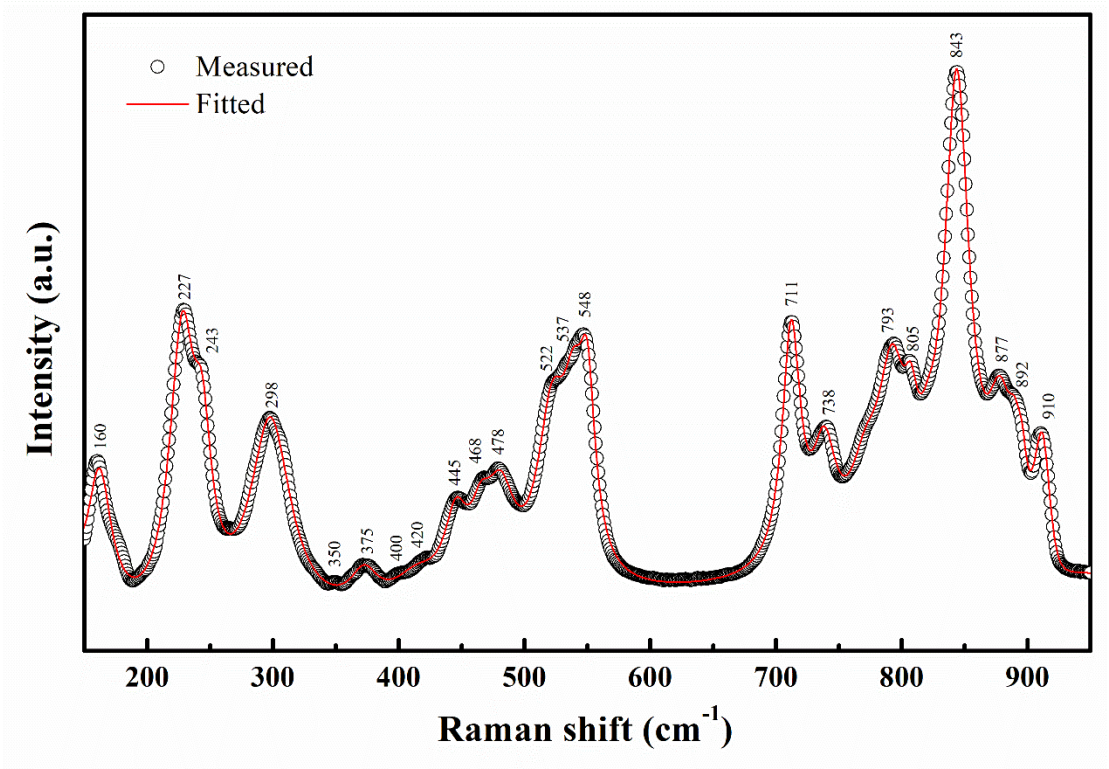

Figure 3

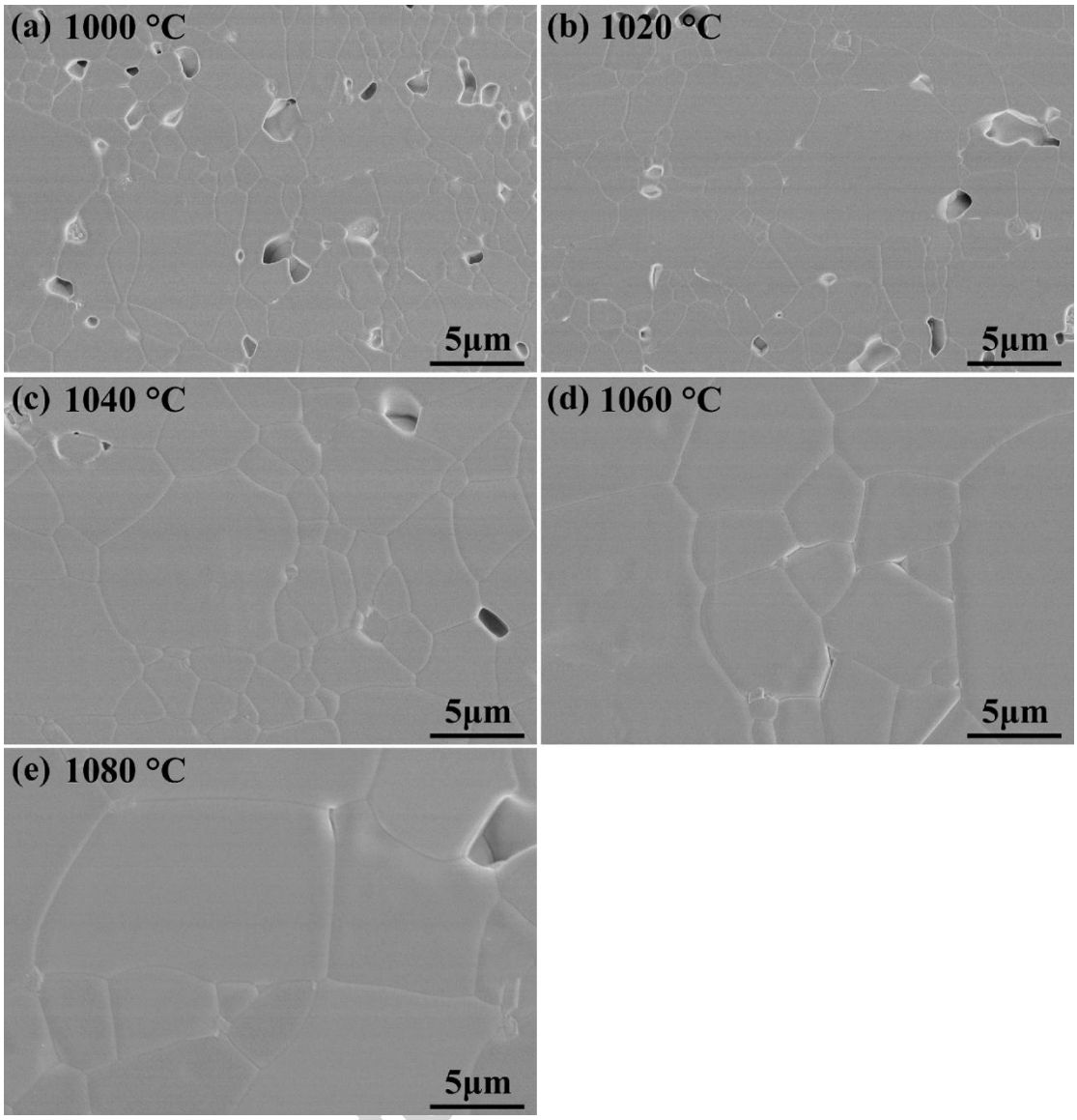

Figure 4

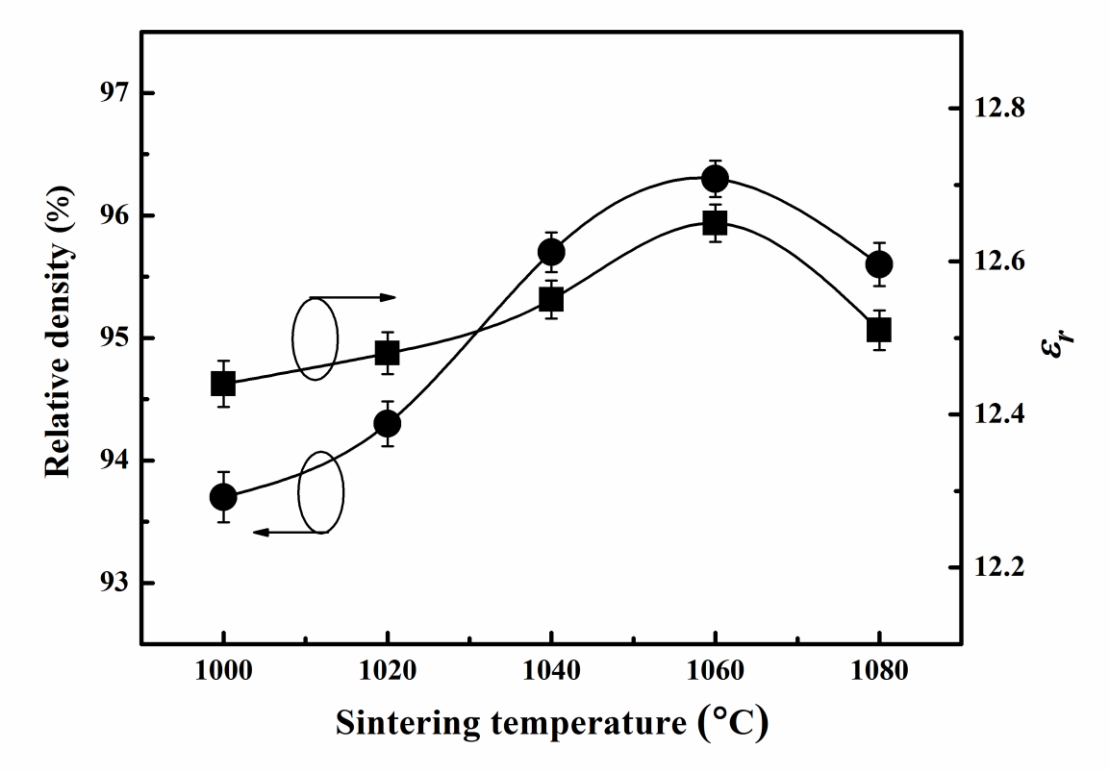

Figure 5

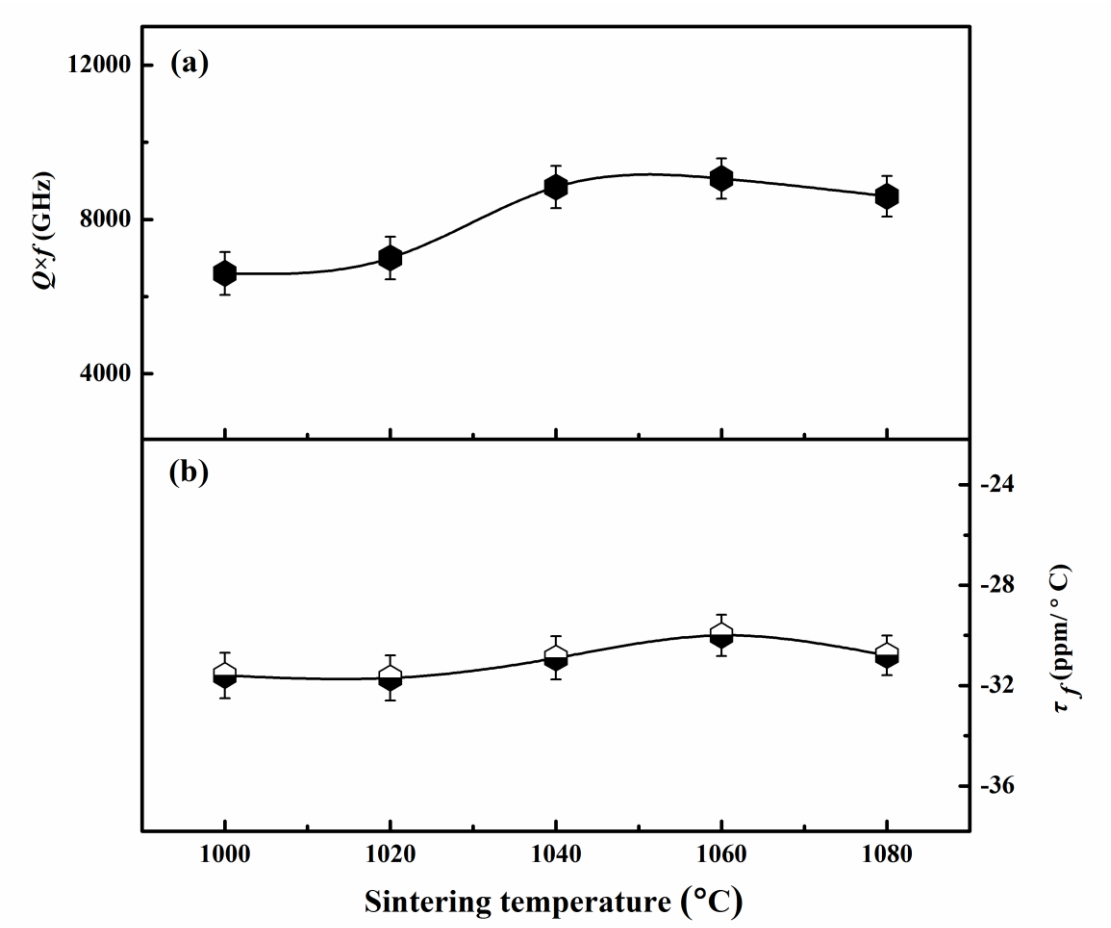

Figure 6

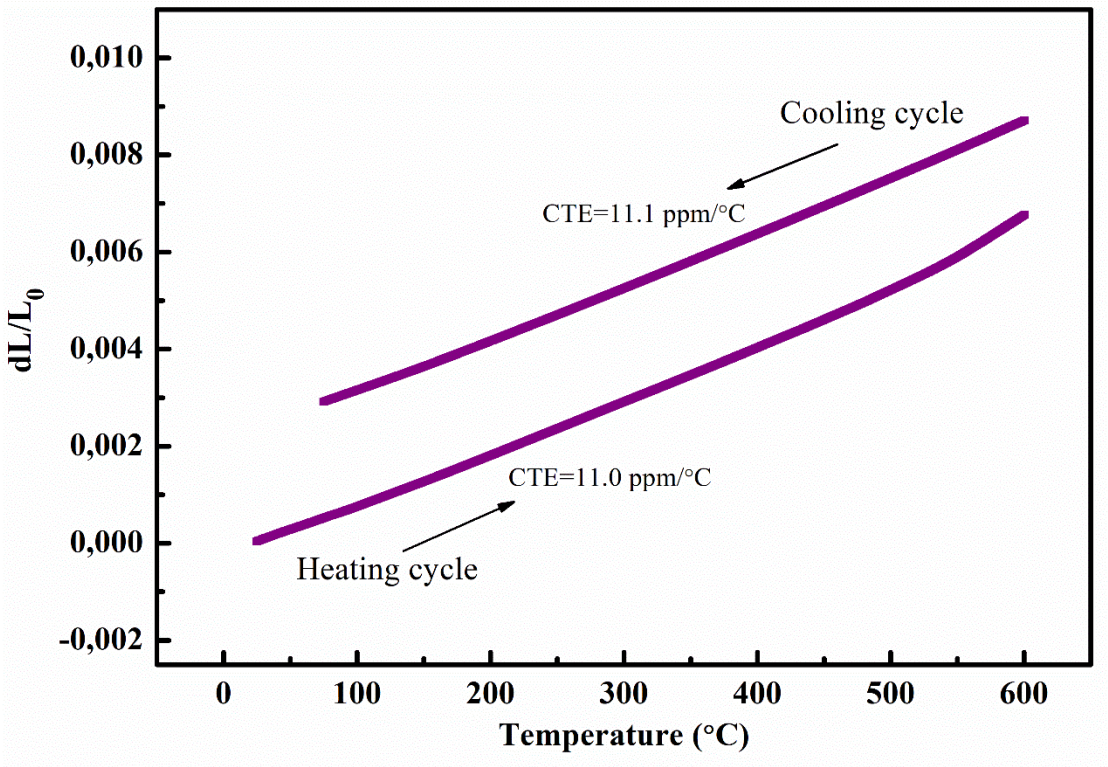

Figure 7

Table 1 The atomic coordinates of $Ba_2Ge_2TiO_8$ and the reliability factors

Atom	Site	x/a	y/b	z/c	B_{iso} (Å^2)	Occupancy
Ba(1)	4e	0	0.3273(8)	0	1.0508(1)	0.5
Ba(2)	4d	0.1730(4)	0	0	1.0368(7)	0.5
Ge(1)	4e	0	0.1274(5)	0.4911(3)	1.0371(5)	0.5
Ge(2)	4d	0.3639(9)	0	0.4825(9)	1.1351(2)	0.5
Ti(1)	4c	0.25	0.25	0.4697(9)	1.2821(1)	0.5
O(1)	8f	0.1076(1)	0.1922(3)	0.3632(7)	0.7379(9)	0.5
O(2)	2a	0	0	0.3652(4)	0.8864(7)	0.25
O(3)	4e	0	0.1266(2)	0.8110(5)	0.6058(1)	0.5
O(4)	8f	0.3086(7)	0.1143(4)	0.3452(2)	1.2277(1)	1
O(5)	2b	0	0.5	0.3452(3)	0.6049(9)	0.25
O(6)	4d	0.3754(7)	0	0.8075(6)	1.3728(5)	0.5

O(7)	4c	0	0	0.7823(4)	1.4413(5)	0.5

Table 2 Microwave dielectric properties of $Ba_2TiGe_2O_8$ and BaO-TiO_2 system ceramics

Ceramics	S.T. (°C)	ε_r	$Q\times f$ (GHz)	τ_f (ppm/°C)	Reference
$Ba_2TiGe_2O_8$	1060/4h	12.7	9,060	–30	This work
$BaTi_4O_9$	1350/2h	37	22,700	+15	[30]
$BaTi_4O_9$-citrate route	1250/10h	36	50,500	+16	[31]
$BaTi_4O_9$-co-precipitation	1300/2h	38	28,000	+11	[32]
$BaTi_4O_9$-polymer precursor route	1250/3h	35.6	42,000	+12	[33]
$BaTi_5O_{11}$	1120/48h	42	61,110	+39	[34]
$Ba_2Ti_9O_{20}$	1400/3h	39.8	32,000	+2	[1]